Nanoscale

PAPER

View Article Online
View Journal | View Issue

Cite this: *Nanoscale*, 2024, **16**, 13945

Thermo-optics of gilded hollow-core fibers†

Denis S. Kolchanov, ‡[a] Andrey Machnev,*‡[a] Alexandra Blank,‡[a] Hani Barhom, [a,b] Liangquan Zhu,[c] Qijing Lin,[c] Alexandra Inberg,[a] Kristina R. Rusimova,[d] Mariia A. Mikhailova,[e] Alexander Gumennik, [f] Toms Salgals,[g] Vjačeslavs Bobrovs,[g] Ventsislav K. Valev,[d] Peter J. Mosley[d] and Pavel Ginzburg[a]

Received 20th October 2023,
Accepted 6th May 2024

DOI: 10.1039/d3nr05310e

rsc.li/nanoscale

Hollow core fibers, supporting waveguiding in a void, open a room of opportunities for numerous applications owing to an extended light–matter interaction distance and relatively high optical confinement. Decorating an inner capillary with functional materials allows tailoring the fiber's optical properties further and turns the structure into a functional device. Here, we functionalize an anti-resonant hollow-core fiber with 18 nm-size gold nanoparticles, approaching a uniform 45% surface coverage along 10 s of centimeters along its inner capillary. Owing to a moderately low overlap between the fundamental mode and the gold layer, the fiber maintains its high transmission properties; nevertheless, the entire structure experiences considerable heating, which is observed and quantified with the aid of a thermal camera. The hollow core and the surrounding capillary are subsequently filled with ethanol and thermo-optical heating is demonstrated. We also show that at moderate laser intensities, the liquid inside the fiber begins to boil and, as a result, the optical guiding is destroyed. The gilded hollow core fiber and its high thermal-optical responsivity suggest considering the structure as an efficient optically driven catalytic reactor in applications where either small reaction volumes or remote control over a process are demanded.

I. Introduction

Photonic crystal fibers (PCFs) are a special class of waveguiding devices, which support long-range optical propagation, owing to the microstructure periodic internal geometry of glass capillaries. Similarly to standard telecommunication fibers, light guiding in solid-core PCFs occurs in a higher index medium. Hollow-core fibers (HCFs), however, enable light propagation in a void,[1] opening pathways for new strategies in tailoring light–matter interactions. The holes within HCFs can be filled with liquids or gases for sensing purposes, or the inner surfaces functionalized with a variety of materials to provide the fiber with additional capabilities on top of light guiding. Interaction efficiencies in these scenarios are achieved owing to the overlap between an analyte and a confined mode, propagating along a fiber. Complex inner design together with various guiding mechanisms allowed the demonstration of a range of practical devices, including polarization filters,[2] beam splitters,[3] logic gates, lasers,[4] and sensors.[2,5–10] Among a variety of applications, inner-core functionalization strategies have been increasingly explored.[1,6,11–14] While many different materials, including nanostructures, have been explored in this endeavor,[15–17] here we will concentrate on plasmonic metals, which are known for their capabilities to manipulate light below the classical diffraction limit.[17,18] Functionalization of hollow-core PCFs with silver and gold nanoparticles has been demonstrated.[1–3,12,15] The surface plasmon resonance phenomenon inside the fiber was exploited and considered for sensing. Surface-Enhanced Raman Spectroscopy (SERS)-based detection was found to be particularly efficient, underlining the benefit of an extended light–matter interaction length along the fiber.[11,17] PCF-based chemical sensing, enhanced by plasmonic phenomena, is comprehensively reviewed in ref. 19.

Due to its high optical confinement within a compact volume, a hollow-core Photonic Crystal Fiber (HC-PCF) emerges as a highly promising platform for probing photocatalytic reactions.[20] This architecture has been effectively employed in various studies, such as analyzing the photo-

[a]*Department of Electrical Engineering, Tel Aviv University, Ramat Aviv, Tel Aviv, 69978, Israel. E-mail: andreym@mail.tau.ac.il*
[b]*Israel Triangle Regional Research and Development Center, Kfar Qara' 3007500, Israel*
[c]*State Key Laboratory for Manufacturing Systems Engineering, Xi'an Jiaotong University, Xi'an 710054, China*
[d]*Center for Photonics and Photonic Materials, Department of Physics, University of Bath, Bath BA2 7AY, UK*
[e]*Department of Materials Science and Engineering, Faculty of Engineering, Tel Aviv University, Tel Aviv 69978, Israel*
[f]*Department of Intelligent Systems Engineering, Luddy School of Informatics, Computing, and Engineering, Indiana University Bloomington, Bloomington, IN, USA*
[g]*Institute of Telecommunications, Riga Technical University, Riga, Latvia*
†Electronic supplementary information (ESI) available. See DOI: https://doi.org/10.1039/d3nr05310e
‡Equal contribution.

redox-catalyzed α-C–H alkylation of primary alkylamines using HC-PCF microreactors,[21] investigating graphitic, N-doped, and amorphous carbon-nanodots for photocatalytic fuel production,[22] enhanced photolysis reactions in toluene using HC-PCF made from high-index soft glass[23] and measuring the quantum yield of vitamin B12 conversion in a liquid-filled HC-PCF.[24] These studies not only validate the suitability of PCF fibers in photocatalysis, but also contribute significantly to the understanding of photocatalytic mechanisms, paving the way for more in-depth investigations into chemical processes. This approach has been explored in several configurations, where gold and silver nanoparticles were in use.[25–27]

Gold's chemical inertness and resistance to oxidation are key attributes that ensure the durability and functional integrity of its coatings, particularly in diverse chemical environments. Gold nanoparticles can efficiently absorb and scatter light at wavelengths, corresponding to their localized plasmon resonances. Plasmonic nanoparticles can also promote catalytic reactions, though the topic remains debatable.

The field of plasmonic catalysis, especially with gold nanoparticles, is drawing significant interest. Studies demonstrate that localized surface plasmon resonance in gold nanoparticles can facilitate CO disproportionation at room temperature, highlighting the potential of plasmonic nanostructures in catalysis.[28] Furthermore, the effectiveness of gold, silver, and copper plasmonic nanoparticles in enhancing catalytic processes under visible light has been noted, underscoring the broad applicability of plasmon-mediated catalysts in various light-driven reactions.[29] In many scenarios, reaction rates depend on local temperature, which can be controlled with the aid of plasmonic absorption.[30,31] In this case, the interaction has to be tailored in order to efficiently distribute the temperature along at least several centimeters of a fiber. In other words, the plasmonic layer must be sufficiently absorptive to induce heating, but not too absorptive to dissipate the entire light intensity close to the fiber facet.

Here, we demonstrate the design and realization of a plasmonic coating, which allows the HCF to be heated by light propagating in its core over lengths up to tens of centimeters. The fabrication process is described and then followed by optical characterization of the structure – the gilded fiber. Both air and liquid-filled scenarios are considered, demonstrating efficient heating, mapped using a thermal camera. Owing to the efficiency of this process, the temperature of the liquid inside the core can be elevated toward its boiling point. When reached, bubbles form high-contrast inclusions within the fiber core and scatter the propagating light, leading to a drop in optical transmission. Boiling scenarios are primarily summarized in movies, which appear in the ESI.†

II. Gilded fiber – fabrication

The fiber was fabricated using the stack-and-draw technique, specifically designed to significantly suppress higher-order modes. This type of fiber is known as a one-ring or negative curvature photonic crystal fiber. It features a hollow core, which is created by several capillaries that extend along the entire length of the fiber. The diameter of the fiber is approximately 30 microns.[32] The HCF has a low-loss transmission window for wavelengths around 600 nm.

The process to coat the inside of the HCF with gold nanoparticles encompasses two main steps – (i) synthesis of monodispersed small gold nanoparticles (Au NPs) and (ii) inner core functionalization with the aid of colloidal chemistry techniques.

Au NPs were synthesized by the citrate method, based on the chemical reduction of Au^{3-} with a trisodium citrate solution.[33] Briefly, a three-neck reflux flask was filled with 100 ml of deionized water and brought to a boil with constant stirring with a 350 rpm magnetic stirrer. Then 1 ml of HAuCl4 (2.5 mmol) and immediately 250 μl of trisodium citrate solution (0.334 mol) were added. After 1 minute, the solution turned blue, and after 5 minutes the color changed to red orange, the flask was removed from the stove and cooled in air. The hydrodynamic particle diameter was checked using the dynamic light scattering (DLS) method using a Zetasizer Nano ZS from Malvern Analytical. Particles with 18 nm mean diameter and 5 nm standard deviation value were found.

The inner surface of the fiber was coated with Au NPs using a three-stage chemical treatment. A silicone fiber was hermetically connected to the syringe pump to perform the procedure, described below. The first step was to treat the fiber with a 35% HNO_3 solution for 20 minutes to clean and activate the glass surface, after which the fiber was washed with deionized water (DIW) for 5 minutes until a neutral pH was reached. The second step was the salinization of the surface using a 2% solution of (3-aminopropyl)trimethoxysilane (APTMS) in ethyl alcohol (EtOH) for 20 min to create amino groups on the glass surface that bind gold nanoparticles. After salinization, the fiber was thoroughly washed with EtOH and DIW for 5 min. The final stage was pumping through the fiber of the colloidal gold solution obtained after synthesis for 20 min. For the correct course of the reaction, it is necessary to change the syringe to avoid the coagulation of gold in its volume. Upon completion of the experiment, the fiber was successively washed with DIW, EtOH, dried in an airstream, and annealed in a muffle furnace at 500 °C for 5 minutes. The heating rate of the furnace was 10 °C min^{-1}.

To determine the filling factor of the HCF with gold, the estimation was performed by binarizing SEM images and calculating the ratio of the area occupied by white pixels (representing gold particles) to the total area of the processed image. In all the experiments we used HCFs with their inner walls coated with a thin layer of gold nanoparticles (hydrodynamic size 18 nm). Fig. 1 shows a scanning electron microscopy (SEM) image of the gold-coated fiber cross-section, where gold nanoparticles are seen to uniformly cover the inner surface of the fiber without blocking the core thus leaving air and liquid passage through it. To verify the uniformity of the coverage along the fiber, a long 10 cm section was cut into pieces and each one was analyzed independently. Fig. 1(c) demonstrates

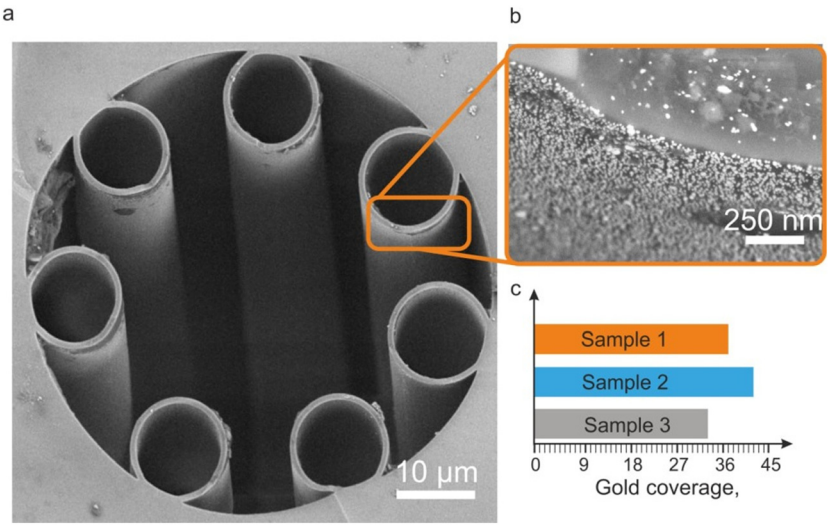

Fig. 1 (a) SEM image of the HCF with a gold nanoparticle layer deposited on its inner walls. (b) Back scattering electrons (BSE) image of a magnified inner wall surface of a gold-coated fiber; bright spots are Au NPs. (c) Averaged surface coverage of the inner surface of the capillary by Au NPs for 3 different cuts along the fiber.

the surface coverage for 3 samples, which all possess a similar 35% coverage with several percent deviation, thus confirming the uniformity over a long sample.

III. Gilded fiber – optical characterization

To characterize the optical properties of the samples, a transmission setup has been constructed (Fig. 2(a)). A YSL-Pro supercontinuum laser was used, providing light with ~300 ps pulse duration and a total output power of 80 mW. The output beam from the supercontinuum is filtered by a dichroic mirror to the 500–650 nm range and then coupled to the hollow core photonic crystal fiber. For analyzing the spectral and mode content of the fiber, the light is imaged on a CCD camera and coupled to the spectrum analyzer (Avantes AvaSpec-2048L). The setup enables measuring the transmission spectrum of the fiber.

Liquid filling of the fiber is carried out by using a specially designed liquid cell (LC in Fig. 2(a)). The inlet of the cell is connected to a syringe *via* thin plastic tubing. Using the syringe, ethanol (or any other liquid) is delivered to the cell and goes through the fiber due to the pressure created by the syringe plunger. The cell has a transparent glass window allowing laser coupling to the fiber facet, which is sealed into the cell.

Ethanol, a widely used organic solvent with a relatively low boiling point (approximately 78 °C) and low surface tension (25 mN m^{-1} at 25 °C), was selected for its ability to remove air bubbles from the core of PCF-fiber. Additionally, ethanol is suitable for investigating catalytic reactions. Research has

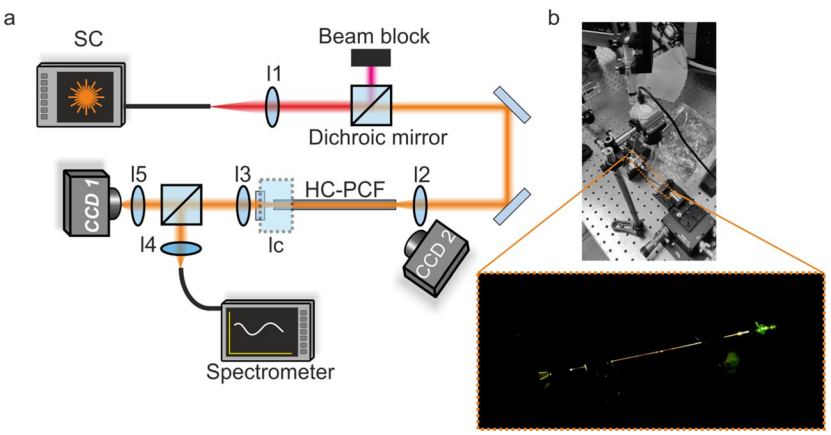

Fig. 2 (a) Scheme of the experimental setup. (b) Photograph of the setup. Inlet – a photograph of the light, scattered from the ethanol-filled hollow-core gilded fiber.

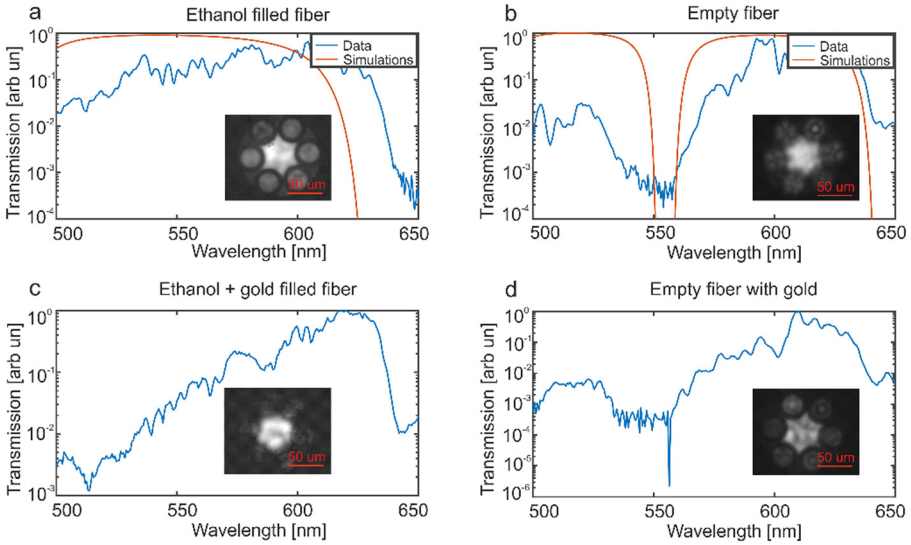

Fig. 3 Transmission (arbitrary units) spectra of fibers. (a,b) for ethanol and air filled fibers. (c,d) for ethanol and air filled gilded fibers correspondingly. Insets – the CCD image of the optical mode (overall light intensity in the 500–650 nm spectral range).

examined the photo-thermal catalytic reactions of ethanol over Ag/TiO2, highlighting the role of plasmonic resonance in enhancing reaction kinetics.[34] The second end of the fiber is free, and the liquid can flow out. While for this study the leakage does not cause any constraint owing to a very small outlet flow, it can be blocked, if necessary, by introducing another liquid cell. Fig. 2(b) shows the photograph of the setup, positioned on an optical table. Fig. 2(b, inset) shows the photograph of the light-guiding ethanol-filled gilded fiber. The light scattering is quite uniform, thus supporting the claim of uniform coverage with Au NPs. Also, the overall transmission through the system is about 30%, thus allowing the assessment of the guided mode spectrum and other parameters, as will be demonstrated hereinafter.

Transmission characteristics of the pure and gilded fibers have been measured for both air and ethanol-filled conditions, using the setup described above. Comparing the performance of the empty and ethanol-filled pure fibers (Fig. 3(a and b)), a red shift of the transmission window, induced by the liquid, can be noted. The experiments were performed with 20 cm long sections. Since the sample is rather short, nonvanishing transmission is observed even at wavelengths where the HCF loss is high. The infinite fiber behavior can be predicted with a numerical model.[30] The approach is to represent the complex inner structure of the fiber with a simple concentric layer with thicknesses equal to the wall thickness of the smaller capillary (7 smaller tubes in Fig. 1(a)) and the refractive index of fused silica. This approach was found to replicate the guiding properties of the one-ring fiber quite accurately and allows us to model the impact of materials, which fill the inner capillary. However, the model faced challenges in approximating the gilded fiber behavior, due to the large number of free parameters.

Numerical predictions appear as red solid curves in Fig. 3(a and b) and resemble the experimental data. Transmission characteristics of the gilded fiber appear in Fig. 3(c and d). On comparing empty fibers (pure *vs.* gilded – panels a and c), an additional attenuation near 500–530 nm appears owing to the plasmonic resonance. This result confirms the claim that the light interaction with Au NPs is considerable, nevertheless it is not overwhelming, which is important for uniform heating of the fiber. The introduction of ethanol into the gilded fiber smears the plasmonic peak, which has to shift to longer wavelengths by ~20 nm (the assessment is done with Mie solutions, applied to an 18 nm gold sphere in a host medium – *i.e.*, air *vs.* ethanol).

In all the experiments, the optical mode at the output facet of the fibers was imaged using the CCD camera and the results are given in the insets to Fig. 3. In all cases, the excitation of a mixture of modes was observed, which could be due to the fiber's limited length or the enhanced losses resulting from the introduction of gold filling. The light is primarily confined in the void, having a relatively small overlap with the gilded capillaries.

IV. Temperature profiles

The temperature distributions along the fibers were measured with a thermal camera (ICI 8640 S). Fig. 4 summarizes the results, obtained with empty fibers (air-filled, without ethanol). Responses of the gilded fiber are shown in the upper row in Fig. 4, while the bottom row shows the reference measurement. The excitation was performed with the supercontinuum laser (as in the set of transmission experiments). The laser was filtered to the range of 500–600 nm to match the plasmon resonance of the gold nanoparticles and underline the differences between the fibers. The experiments were performed with 3 different laser intensities, measured using a

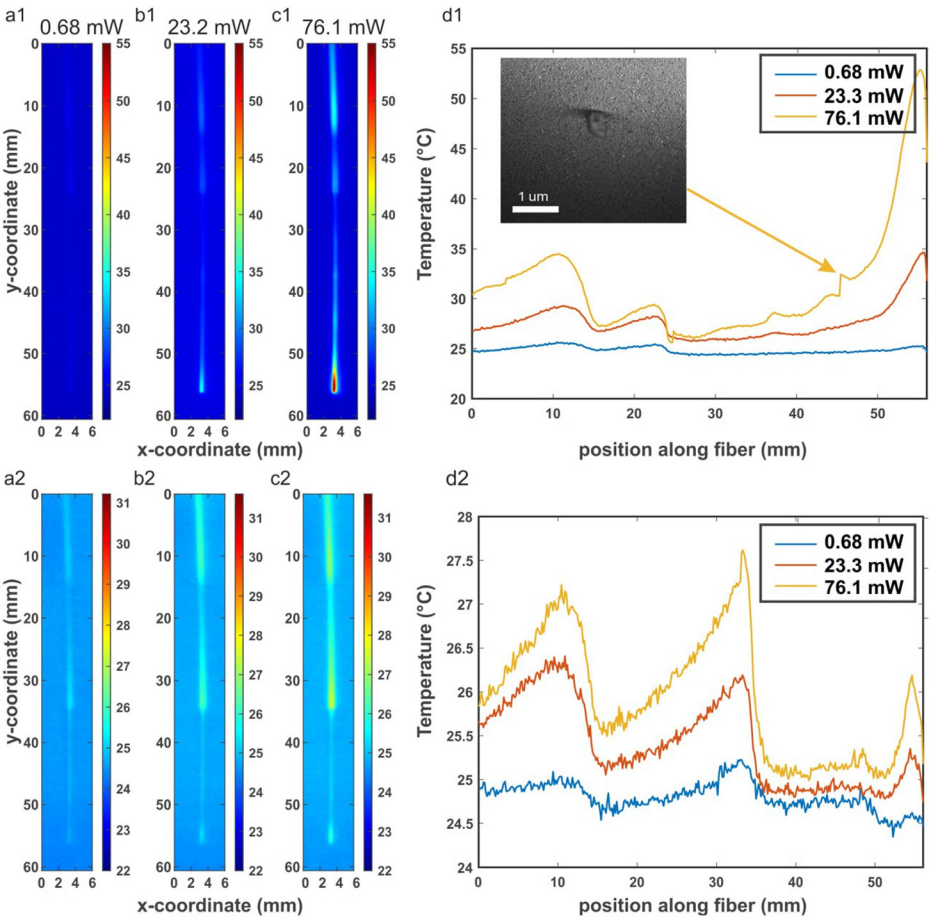

Fig. 4 Temperature distribution along ordinary and gilded air-filled HCFs. The laser is launched from the bottom facet. The top row (a1, b1 and c1) – gilded fiber. Input laser powers are indicated on the plots. The bottom row – (a2, b2 and c2) the ordinary fiber, the same laser parameters. Panels d1 and d2 are the cuts of the colormaps.

power meter before launching the light into the system. Since the coupling efficiencies are power-independent but unknown, the powers indicated in the figure legends can be only considered relative to each other. In the colormaps, the laser is launched from the lower face, and on the 1D plots, demonstrating the cuts through the fiber center, the input is on the left side (60 mm, *x*-axis).

The reference measurement with the uncoated HCF demonstrates minor fluctuations in the temperature, approaching 2 °C for the maximal power of 76.2 mW. Two spikes in the temperature distribution appear along the fiber and these are points where excess scattering occurs in the HCF owing to the imperfections in the HCF or contamination. For an additional assessment, a black marker spot on the fiber cladding also leads to a local temperature elevation.[35] While only a minor temperature rise was observed with the ordinary fiber sample, the gilded fiber demonstrates significant heating. During the fabrication and handling process, the fiber ends are susceptible to microscopic damage, which can lead to irregularities in the fiber's structure. These imperfections can disrupt the uniformity of light propagation within the fiber, resulting in localized heating and, consequently, the observed temperature spikes Fig. 4(d1 and d2) at 56 mm. In the case of gilded fibers, the presence of gold nanoparticles might exacerbate this effect due to their high light absorption and heat conversion efficiency. Up to 30 °C difference from the ambient temperature has been observed. The temperature along the fiber drops nearly exponentially. This can be attributed to the fact that a large proportion of the light is not being coupled to the fiber mode and has a strong overlapping with the gold layer and/or fiber walls. Several areas with spiky behavior along the fiber are observed and, similarly to the ordinary fiber, are attributed to scattering centers caused by imperfections in the HCF or the coating, Fig. 4(d1). Fiber was fixed by using transparent tape, to prevent fiber shaking due to the air flows, which might result in additional losses and appearing of the correlated hot spots.

V. Boiling inside the gilded fiber

The next step was to fill the fiber with ethanol and retrieve the temperature. The available light intensity of the supercontinuum laser in the visible range is insufficient to reach the boiling point of the liquid inside the gilded fiber. For this

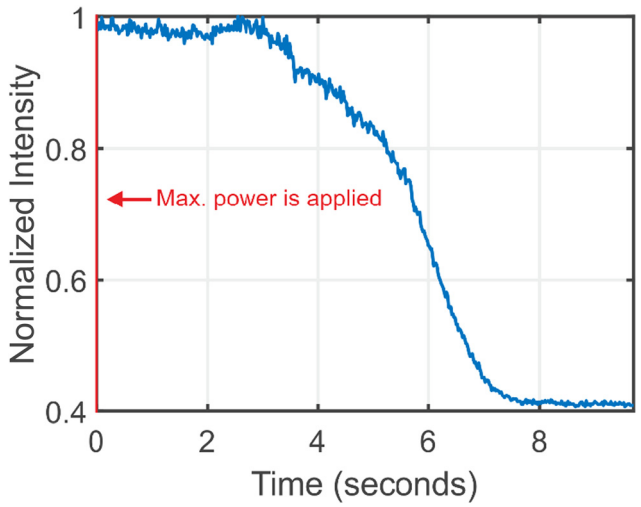

Fig. 5 Normalized transmission signal measured at the output end of the fiber using a CCD camera in time.

purpose, the previously filtered IR spectral part (the supercontinuum pump) was unblocked and launched into the fiber. Ethanol, however, has a significant absorption in the IR region[36] and is also subject to effective laser heating. During the experiment, boiling was achieved (movies are in the ESI†). An excessive generation of bubbles caused a significant light scattering and, as a result, boiling was observed only close to the input facet (Visualization 1). On Visualization 2 the output fiber facet was imaged on the CCD camera (THORLABS, Digital camera) and a supercontinuum (YSL-SC Pro) was coupled to the fiber from the opposite end facet, then the output power of the laser was gradually increased. At about 97 mW (in the visible region), the output signal started dropping and reached its minimum for about 7.6 seconds (Fig. 5).

Boiling within a fiber represents a critical challenge for photo-catalytic processes, primarily because it significantly increases laser scattering, thereby hindering the passage of the laser beam through the fiber. This phenomenon, however, also indicates the capability of the system to reach temperatures exceeding the boiling point of solvents like ethanol. This observation suggests the potential for conducting reactions under high-temperature or high-pressure conditions, provided that appropriate modifications are made to the experimental setup. Such modifications could involve enhancing the thermal and pressure resistance of the fiber, as well as optimizing the laser and photo-catalytic system to control and withstand these extreme conditions. By doing so, it opens the possibility of exploring a wider range of chemical reactions, some of which may only be feasible at temperatures or pressures above the boiling point of common solvents.

VI. Conclusion

A gilded hollow-core fiber architecture has been introduced and investigated both in terms of optical and thermo-optical properties. The samples were fabricated with the aid of colloidal chemistry, where the inner capillary of the fiber has been washed with 18 nm gold nanoparticles in a solution. As a result, uniform nanoparticle layers, with controllable surface coverages, reaching 40%, have been obtained. Optical transmission of gilded fibers with air and ethanol-filled cores has been characterized, demonstrating a moderate interaction between light and plasmonic particles. This balance supports long-range optical propagation on one hand and enables heating the surface on another. As a result, the fiber has been shown to acquire a temperature increase over 10 s of centimeter sections. Temperature mapping of the fiber has been done with a thermal camera, and 10 s of degrees of heating have been shown, opening pathways to promote light-driven catalytic reactions. As an outlook, liquid boiling inside the fiber has been discussed and demonstrated. Owing to significant light scattering on the bubbles, uniform boiling inside the core is not possible with a propagating mode, which motivates developing other strategies for boiling, *e.g.*, at transverse illumination over a large field of view.

As an outlook, given a higher energy throughput, gilded hollow core fibers are promising candidates for laser-ignition delivery in internal combustion engines. Laser ignition has advantages over the electrical spark plug due to the reduced combustion duration and simultaneous multipoint combustion[37] achieved with appropriate end-facet diffractive optics, resulting in faster energy release and thus higher thermal efficiency, becoming one of the only ways for igniting the leaner or higher-pressure fuel-air mixtures.[38] Hollow core fibers enable a tight light focusing on the output ignition spot, as well as capable of delivering wavelengths, effective in creating an ignition spark, but unsupported by the solid-core fibers due to high absorption, such as mid-infrared, on the other hand, are extremely sensitive to bending loss, if uncoated, or prone to speckling, both longitudinal and transverse, when fully coated. This speckling, resulting from a random constructive multi-modal interference, causes ignition misfires and can damage the fiber itself.[39] The gilded fiber potentially targets problems arising from both extremes. On the one hand, its lower modes are less sensitive to bending loss than in uncoated fibers. On the other hand, fewer modes supported over longer lengths than in the fully coated fiber to prevent significant speckling.

Conflicts of interest

The authors declare no conflicts of interest.

Acknowledgements

The TAU team was supported by ERC StG 'In Motion' (802279). The team acknowledges QuanTAU – Center for Quantum Science and Technology equipment grant, and research was

supported by the RRF project Latvian Quantum Technologies Initiative Nr. 2.3.1.1.i.0/1/22/I/CFLA/001.

References

1 A. Schwuchow, M. Zobel, A. Csaki, K. Schröder, J. Kobelke, W. Fritzsche and K. Schuster, Monolayers of different metal nanoparticles in microstructured optical fibers with multiplex plasmonic properties, *Opt. Mater. Express*, 2012, **2**(8), 1050–1055.

2 M. M. Rahman, A. Khaleque, M. T. Rahman and F. Rabbi, Gold-coated photonic crystal fiber based polarization filter for dual communication windows, *Opt. Commun.*, 2020, **461**, 125293.

3 N. Gómez-Cardona, C. Jiménez-Durango, J. Usuga-Restrepo, P. Torres and E. Reyes-Vera, Thermo-optically tunable polarization beam splitter based on selectively gold-filled dual-core photonic crystal fiber with integrated electrodes, *Opt. Quantum Electron.*, 2021, **53**(2), 68.

4 M. R. A. Hassan, F. Yu, W. J. Wadsworth and J. C. Knight, Cavity-based mid-IR fiber gas laser pumped by a diode laser, *Optica*, 2016, **3**(3), 218–221.

5 M. De, T. K. Gangopadhyay and V. K. Singh, Prospects of photonic crystal fiber for analyte sensing applications: an overview, *Meas. Sci. Technol.*, 2020, **31**(4), 42001.

6 B. Doherty, A. Csáki, M. Thiele, M. Zeisberger, A. Schwuchow, J. Kobelke, W. Fritzsche and M. A. Schmidt, Nanoparticle functionalised small-core suspended-core fibre – a novel platform for efficient sensing, *Biomed. Opt. Express*, 2017, **8**(2), 790–799.

7 T. Gong, Y. Cui, D. Goh, K. K. Voon, P. P. Shum, G. Humbert, J.-L. Auguste, X.-Q. Dinh, K.-T. Yong and M. Olivo, Highly sensitive SERS detection and quantification of sialic acid on single cell using photonic-crystal fiber with gold nanoparticles, *Biosens. Bioelectron.*, 2015, **64**, 227–233.

8 M. A. Jabin, Y. Luo, G.-D. Peng, M. J. Rana, K. Ahmed, T. K. Nguyen, B. K. Paul and V. Dhasarathan, Design and fabrication of amoeba faced photonic crystal fiber for biosensing application, *Sens. Actuators, A*, 2020, **313**, 112204.

9 A. Gumennik, A. M. Stolyarov, B. R. Schell, C. Hou, G. Lestoquoy, F. Sorin, W. McDaniel, A. Rose, J. D. Joannopoulos and Y. Fink, All-in-Fiber Chemical Sensing, *Adv. Mater.*, 2012, **24**(45), 6005–6009.

10 A. M. Stolyarov, A. Gumennik, W. McDaniel, O. Shapira, B. Schell, F. Sorin, K. Kuriki, G. Benoit, A. Rose, J. D. Joannopoulos and Y. Fink, Enhanced chemiluminescent detection scheme for trace vapor sensing in pneumatically-tuned hollow core photonic bandgap fibers, *Opt. Express*, 2012, **20**(11), 12407–12415.

11 M. Pisco, A. Cusano and A. Cutolo, *Photonic Bandgap Structures Novel Technological Platforms for Physical, Chemical and Biological Sensing*, Bentham Science Publishers, 2012.

12 Y. Xu, X. Zhang, X. Zhu and Y. Shi, Surface plasmon resonance sensor based on gold-coated hollow fiber structure, in *Twelfth International Conference on Information Optics and Photonics*, ed. Y. Yang, SPIE, 2021, p. 194.

13 T. Ermatov, R. E. Noskov, A. A. Machnev, I. Gnusov, V. Atkin, E. N. Lazareva, S. V. German, S. S. Kosolobov, T. S. Zatsepin, O. V. Sergeeva, J. S. Skibina, P. Ginzburg, V. V. Tuchin, P. G. Lagoudakis and D. A. Gorin, Multispectral sensing of biological liquids with hollow-core microstructured optical fibres, *Light: Sci. Appl.*, 2020, **9**(1), 173.

14 N. Kaydanov, S. Perevoschikov, S. V. German, S. A. Romanov, T. Ermatov, A. A. Kozyrev, J. Cvjetinovic, A. Machnev, R. E. Noskov, S. S. Kosolobov, J. S. Skibina, A. G. Nasibulin, C. Zakian, P. G. Lagoudakis and D. A. Gorin, Optoacoustic Effect in a Hybrid Multilayered Membrane Deposited on a Hollow-Core Microstructured Optical Waveguide, *ACS Photonics*, 2021, **8**(11), 3346–3356.

15 T. Ermatov, Y. V. Petrov, S. V. German, A. A. Zanishevskaya, A. A. Shuvalov, V. Atkin, A. Zakharevich, B. N. Khlebtsov, J. S. Skibina, P. Ginzburg, R. E. Noskov, V. V. Tuchin and D. A. Gorin, Microstructured Optical Waveguide-Based Endoscopic Probe Coated with Silica Submicron Particles, *Materials*, 2019, **12**(9), 1424.

16 T. Ermatov, J. S. Skibina, V. V. Tuchin and D. A. Gorin, Functionalized Microstructured Optical Fibers: Materials, Methods, Applications, *Materials*, 2020, **13**(4), 921.

17 D. K. Gramotnev and S. I. Bozhevolnyi, Plasmonics beyond the diffraction limit, *Nat. Photonics*, 2010, **4**(2), 83–91.

18 P. Ginzburg, D. Arbel and M. Orenstein, Gap plasmon polariton structure for very efficient microscale-to-nanoscale interfacing, *Opt. Lett.*, 2006, **31**(22), 3288–3290.

19 C. Ren, J. Yuan, K. Wang, B. Yan, X. Sang and C. Yu, Design of Photonic Crystal Fiber Refractive Index Sensor Based on Surface Plasmon Resonance Effect for the Dual-Wavebands Measurement, *Fiber Integr. Opt.*, 2021, **40**(4–6), 263–275.

20 P. Koehler, T. Lawson, J. Neises, J. Willkomm, B. C. M. Martindale, G. A. M. Hutton, D. Antón-García, A. Lage, A. S. Gentleman, M. H. Frosz, P. St.J. Russell, E. Reisner and T. G. Euser, Optofluidic Photonic Crystal Fiber Microreactors for In Situ Studies of Carbon Nanodot-Driven Photoreduction, *Anal. Chem.*, 2021, **93**(2), 895–901.

21 A. S. Gentleman, T. Lawson, M. G. Ellis, M. Davis, J. Turner-Dore, A. S. H. Ryder, M. H. Frosz, M. Ciaccia, E. Reisner, A. J. Cresswell and T. G. Euser, Stern–Volmer analysis of photocatalyst fluorescence quenching within hollow-core photonic crystal fibre microreactors, *Chem. Commun.*, 2022, **58**(75), 10548–10551.

22 P. Koehler, J. Neises, J. Willkomm, T. Lawson, D. Antón-García, M. H. Frosz, P. St. J. Russell, E. Reisner and T. G. Euser, Photoreduction in Optofluidic Hollow-Core Photonic Crystal Fiber, in 2019 Conference on Lasers and Electro-Optics Europe & European Quantum Electronics Conference *(CLEO/Europe-EQEC)* 2019, pp. 1–1.

23 A. M. Cubillas, X. Jiang, T. G. Euser, N. Taccardi, B. J. M. Etzold, P. Wasserscheid and P. S. J. Russell, Photochemistry in a soft-glass single-ring hollow-core photonic crystal fibre, *Analyst*, 2017, **142**(6), 925–929.
24 J. S. Y. Chen, T. G. Euser, N. J. Farrer, P. J. Sadler, M. Scharrer and P. S. J. Russell, Photochemistry in Photonic Crystal Fiber Nanoreactors, *Chem. – Eur. J.*, 2010, **16**(19), 5607–5612.
25 J. R. Adleman, D. A. Boyd, D. G. Goodwin and D. Psaltis, Heterogenous Catalysis Mediated by Plasmon Heating, *Nano Lett.*, 2009, **9**(12), 4417–4423.
26 G. Baffou and R. Quidant, Nanoplasmonics for chemistry, *Chem. Soc. Rev.*, 2014, **43**(11), 3898–3907.
27 P. Christopher, H. Xin and S. Linic, Visible-light-enhanced catalytic oxidation reactions on plasmonic silver nanostructures, *Nat. Chem.*, 2011, **3**(6), 467–472.
28 W.-C. D. Yang, C. Wang, L. A. Fredin, P. A. Lin, L. Shimomoto, H. J. Lezec and R. Sharma, Site-selective CO disproportionation mediated by localized surface plasmon resonance excited by electron beam, *Nat. Mater.*, 2019, **18**(6), 614–619.
29 A. Gellé and A. Moores, Plasmonic nanoparticles: Photocatalysts with a bright future, *Curr. Opin. Green Sustain. Chem.*, 2019, **15**, 60–66.
30 M. Zeisberger and M. A. Schmidt, Analytic model for the complex effective index of the leaky modes of tube-type anti-resonant hollow core fibers, *Sci. Rep.*, 2017, **7**(1), 11761.
31 K. R. Rusimova, D. Slavov, F. Pradaux-Caggiano, J. T. Collins, S. N. Gordeev, D. R. Carbery, W. J. Wadsworth, P. J. Mosley and V. K. Valev, Atomic dispensers for thermo-plasmonic control of alkali vapor pressure in quantum optical applications, *Nat. Commun.*, 2019, **10**, 2328.
32 A. A. Machnev, A. P. Pushkarev, P. Tonkaev, R. E. Noskov, K. R. Rusimova, P. J. Mosley, S. V. Makarov, P. B. Ginzburg and I. I. Shishkin, Modifying light–matter interactions with perovskite nanocrystals inside antiresonant photonic crystal fiber, *Photonics Res.*, 2021, **9**(8), 1462–1469.
33 B. V. Enustun and J. Turkevich, Coagulation of Colloidal Gold, *J. Am. Chem. Soc.*, 1963, **85**(21), 3317–3328.
34 M. A. Nadeem and H. Idriss, Photo-thermal reactions of ethanol over Ag/TiO 2 catalysts. The role of silver plasmon resonance in the reaction kinetics, *Chem. Commun.*, 2018, **54**(6), 5197–5200.
35 O. A. Schmidt, M. K. Garbos, T. G. Euser and P. St. J. Russell, Reconfigurable Optothermal Microparticle Trap in Air-Filled Hollow-Core Photonic Crystal Fiber, *Phys. Rev. Lett.*, 2012, **109**, 024502.
36 Q. Dong, C. Yu, L. Li, L. Nie, D. Li and H. Zang, Near-infrared spectroscopic study of molecular interaction in ethanol-water mixtures, *Spectrochim. Acta, Part A*, 2019, **222**, 117183.
37 S. Azarmanesh and M. Z. Targhi, Comparison of laser ignition and spark plug by thermodynamic simulation of multi-zone combustion for lean methane-air mixtures in the internal combustion engine, *Energy*, 2021, **216**, 119309.
38 M. Tsunekane, T. Inohara, K. Kanehara, T. Taira, M. Tsunekane, T. Inohara, K. Kanehara and T. Taira, Micro-Solid-State Laser for Ignition of Automobile Engines, in *Advances in Solid State Lasers Development and Applications*, IntechOpen, 2010.
39 A. P. Yalin, High power fiber delivery for laser ignition applications, *Opt. Express*, 2013, **21**(106), A1102–A1112.